energies

MDPI

Article

A Numerical Investigation of Enhancing Hydrate Dissociation via Co-Production with Shallow Gas upon a Large-Scale Model

Xin Lei [1,2,*], Weixin Pang [1,2], Qiang Fu [1,2], Yuhua Ma [2], Yang Ge [1,2], Lu Liu [3] and Huiyun Wen [1,2]

[1] State Key Laboratory of Natural Gas Hydrates, Beijing 100028, China
[2] Research Institute of China National Offshore Oil Corporation, Beijing 100027, China
[3] School of Petroleum Engineering, China University of Petroleum (East China), Qingdao 266580, China
* Correspondence: leix2023@163.com

Abstract

Investigations into the production of gas hydrates from marine sediments have demonstrated that commercial viability necessitates a daily gas production rate of 130,000 to 200,000 m^3. However, the second-round trial production in the South China Sea yielded only 28,700 m^3/day, falling short of the rule-of-thumb for economic feasibility. Given the coexistence of natural gas hydrates (NGHs) and shallow gas in the subsurface reservoirs of the South China Sea, a co-production strategy (simultaneously exploiting NGHs and shallow gas) was proposed to reduce costs and enhance production efficiency. In this study, a large-scale, three-dimensional, multi-phase, and multi-component model was established based on the NGHs–shallow gas symbiotic system in the Qiongdongnan Basin. A dual horizontal well configuration was designed to extract NGHs from the hydrate-bearing layer and natural gas from the underlying shallow gas layer. Co-production via dual horizontal wells expanded the hydrate dissociation zone from the near-wellbore region to deeper strata, particularly enhanced the dissociation of NGHs in the region between the two horizontal wells. By the 10th year of simulation, the peak and cumulative volume rate of CH_4 released from hydrate dissociation increased to 3.52 and 1.45 times under the co-production scenario, resulting in a 2.4-fold improvement in NGH recovery efficiency. Sensitivity analyses of bottom hole pressure and length of the horizontal intervals revealed that reducing bottom hole pressure significantly improved the daily and accumulative gas production from hydrate-bearing reservoirs. The length of horizontal intervals emerged as a critical factor influencing the dissociation of NGHs, whereas it had negligible impact on gas production from shallow gas reservoir with satisfied permeability. This study provides insights into optimizing the development of marine hydrate resources via integrated exploitation strategies.

Keywords: natural gas hydrate; shallow gas; three-dimensional model; depressurization; dual horizontal well

Check for updates

Academic Editor: Reza Rezaee

Received: 19 January 2026
Revised: 8 February 2026
Accepted: 17 February 2026
Published: 2 March 2026

Copyright: © 2026 by the authors. Licensee MDPI, Basel, Switzerland. This article is an open access article distributed under the terms and conditions of the Creative Commons Attribution (CC BY) license.

1. Introduction

According to national statistics, 40% to 44.9% consumption of natural gas in China depends on imports [1,2], implying a tense domestic situation in energy resources. Natural gas hydrates (NGHs), as solid, non-stoichiometric compounds of small gas molecules and water, draw great attention for their enormous quantity of resources [3,4]. Even the most conservative estimates suggest that the amount of energy in NGHs surpasses twice that of other types of fossil fuels [5,6]. The efficient production and exploitation of NGHs will hopefully alleviate the tension in the energy crisis.

Worldwide, approximately 90% of NGHs exist in shallow offshore layers under deep marine waters [7]. According to current investigations, the quantity of NGH resources (including disseminated NGHs with unsatisfied economic benefits in near-future development) in the South China Sea (SCS) was estimated to be approximately 10 to 26 $\times$ 10^8 t oil equivalent [8]. The geological investigation and resource exploration in the SCS illuminated two main target regions, the Pearl River Mouth Basin (PRMB) and the Qiongdongnan Basin (QDNB), for their ideal geological, geomorphological, and geochemical conditions for NGH reservoirs [9–16]. In the Shenhu area (southern part of the PRMB), two field trials for NGHs production through a vertical and a horizontal well were carried out in 2017 and 2020, with daily production rates reaching 0.51 $\times$ 10^4 and 2.87 $\times$ 10^4 m^3/day [17,18], respectively. Although the daily and accumulation production rates obtained from the horizontal well surpass the previous field trials in Canada, the USA and Japan [19–21], the rule-of-thumb for commercially viable production rates from offshore gas wells is still hard to achieve [22]. Currently, facilities supporting marine NGHs production are built and in position; the key points for pushing next-step exploitation are technical breakthroughs in improving daily production rates and production cycles.

To improve the efficiency and reduce the costs of NGHs production, comprehensive exploration and exploitation for multi-source gases draws great attention [23]. The latest research from the Guangzhou Marine Geology Survey suggests that NGHs and shallow gas in the Lingshui sag in the QDNB form an overall hydrocarbon system [14,24], where the shallow gas reservoirs below NGH layers provide sources for the formation of NGHs and the NGH layers seal the migration pathways for the underlying gas reservoirs [25]. Considering that the submarine pipe networks and basic facilities in the Lingshui gas fields are already built, the co-production of NGHs and shallow gas hopefully improves the exploitation efficiency of the NGH resources in the QDNB.

The co-production theory for NGHs and shallow gas opened a novel field, and the relevant studies have been mainly carried out through experimental and numerical simulation measures. Yang et al. [26] found that the production efficiency of hydrate was improved by 38.4% with the assistance of the underlying shallow gas through experimental methods. Shi et al.'s [27] laboratory simulated the situation where shallow gas participates in the dissociation process of NGHs; the production behaviors of NGHs production with assistance of shallow gas was 106.64% of producing NGHs alone. Correspondingly, the dissociation rate of NGHs surpasses 54~79% as well. For numerical simulations, Zhao et al. [28] constructed a cylindrical model with a radius of 150 m on the basic well data at site W03 in the QDNB, consisting of a hydrate-bearing layer (75.2 m), an interlayer (48.5 m) and a shallow gas layer (61.0 m). A vertical well penetrated through the hydrate-bearing layer and shallow gas layer, with two perforation intervals in these two layers. The cumulative gas production from co-production was 9.6 times and 1.07 times greater than that of NGHs alone and shallow gas alone, which is consistent with experimental results. Jin et al. [29] numerically investigated a depressurization co-production process of NGHs, associated gas and shallow gas through an individual vertical well, which suggested that the shallow gas contributed the highest gas yields. Moreover, perforations, depressurization rates, permeability, and gas saturation also influence the production rates remarkably.

For pursuing higher recovery rates for NGHs, the utilization of horizontal wells in co-production of multi-resource gases is considered and analyzed in numerical simulations. Cheng et al. [30] simulated the co-production behaviors within 100 days on basic double horizontal wells, and the results reveal that gas production surpasses the commercialization threshold. However, limited by the amount of grids, the numerical model presents as a two-dimensional plane perpendicular to the horizontal interval. On one hand, the pressure,

temperature, and saturation fields parallel to the horizontal interval were not able to be analyzed; on the other hand, the gas recovery could only be estimated as the integral of the perpendicular planes, where the mutual impacts between the adjacent grids along horizontal wells were ignored. Wei et al. [31] compared the co-production processes with vertical and horizontal wells based on COMSOL, Multiphysics indicating that the gas yields obtained from dual horizontal wells were 4.1 times that of a single vertical well. In this model, the ranges for pressure and temperature decline induced by the production through horizontal wells were much wider than that in the situation of a vertical well, and the regions where hydrate dissociated extended deeper into the reservoir. However, the scale of the whole reservoir along the horizontal interval was 100 m, which was inadequate for field production.

To sum it up, the scales in the numerical models mentioned above range from 100 to 300 m in radical or horizontal directions, which are restricted to field situations, thus weakening their applicability in formulating production strategies. As for the dissociation processes of NGHs in low-permeability silty sediments, the dissociated zones are limited and a range of several hundred meters is adequate for analyzing the characteristics of pressure and saturation fields. However, in the Lingshui gas field in the QDNB, some of the shallow gas occurred in sandbodies [25], where the reservoir permeability behaves almost two orders of magnitude greater than that in the NGHs sediments. The transfer conductivity of mass and heat in sandy reservoirs is preferable and enables the depressurization spread to the edges of the sandbody, which means the numerical scales of gas reservoirs influence production behaviors severely. Therefore, to numerically analyze the co-production behaviors of NGHs and shallow gas, not only should the phase changes in NGHs be characterized, but the scales of the gas reservoirs should also be considered. Currently, there lacks large-scale models which are able to calculate hydrate dissociation at a true field scale during the depressurization of shallow gas.

In this work, a large-scale numerical model, based on a gas field in the Lingshui sag in the QDNB, is established using the TOUGH + hydrate simulator to investigate the in situ co-production behaviors of NGHs and shallow gas. The well output of natural gas and hydrate dissociation rates obtained through dual horizontal wells are compared with those from a single vertical well. Additionally, an analysis is conducted to elucidate the factors contributing to the variations in the hydrate dissociation regions. Furthermore, a comprehensive examination of other factors influencing the dissociation of hydrates is conducted in different cases. The primary focus of this research is to demonstrate the feasibility of co-producing natural gas hydrates and shallow gas reservoirs, thereby offering valuable insights for the future development of gas hydrate resources.

2. Approaches and Methods

2.1. Geological Background

The QDNB is a NEE-trending rifted basin developed on the pre-Cenozoic basement, situated at the north slope of the South China Sea [32,33]. In the QDNB, four basic tectonic elements are distributed from north to south, named the northern depression, the central uplift, the central depression and the southern uplift, respectively [34]. Lingshui sag is a secondary structural unit located in the west region of the central depression, trending NE-NEE. The Oligocene Yacheng and Lingshui formations, the Neogene Sanya, Meishan, Huangliu, and Yinggehai formations developed over the pre-Paleogene basement sequentially. The target region in this study is Lingshui X gas field, situated in the east of the Lingshui sag (Figure 1) [28,35–37].

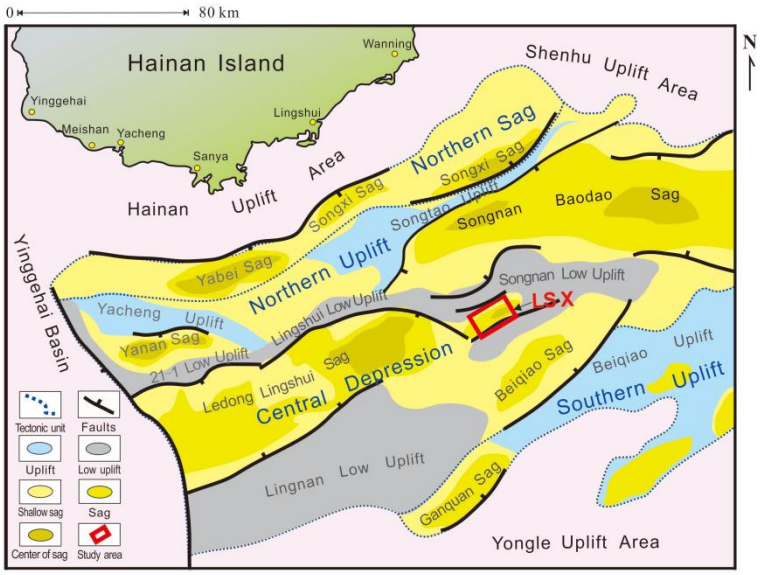

Figure 1. Tectonic unit of the QDNB and study area of the Lingshui area.

The water depth of the target region is 1772 m [30]. The slope of the seafloor is approximately 1.5°, and the geothermal gradients of the region vary from 6.5 to 10.4 °C/hm depending on the distance to gas chimneys. The specific heat of the porous media ranges from 0.91 to 1.4 MJ/m^{3}K. The top of the NGHs reservoir is 122 m below the seafloor, with the NGHs and shallow gas layer having a respective thickness of 58 m and 24 m [30]. The pressure and the temperature of the NGHs reservoir are 18–20 MPa and 14.25–17.16 °C. The hydrate saturation of the main producing horizon ranges from 33% to 55%; other NGH layers only have a hydrate saturation of 3–19%.

2.2. Model Geometry and Domain Discretization

Herein, the NGH sediments and shallow gas layers in the target area are depicted as a three-dimensional cubic model, with five layers and two boundary planes in total (Figure 2). From top to bottom, the model has an overburden layer, NGHs layer, interlayer, shallow gas layer and underlying layer. The total lengths of the cubic model in x, y, z directions are 1500 m, 1500 m and 180 m, respectively. The lengths of all the grids in the x direction are 30 m, while in the y direction, the grids where wells are arranged are narrowed down to 1 m, and increase proportionally with the distance from the horizontal wellbore. In the vertical dimension, the NGHs and shallow gas layer extend 58 m, and 24 m, the interlayer between these two layers has a thickness of 38 m, and the overburden and underlying layers are both 30 m. Near the wellbore and the interfaces of different layers, the grids are also gradually reduced to 1 m. The system of NGHs and shallow gas reservoirs is discretized into 73,920 grids in total.

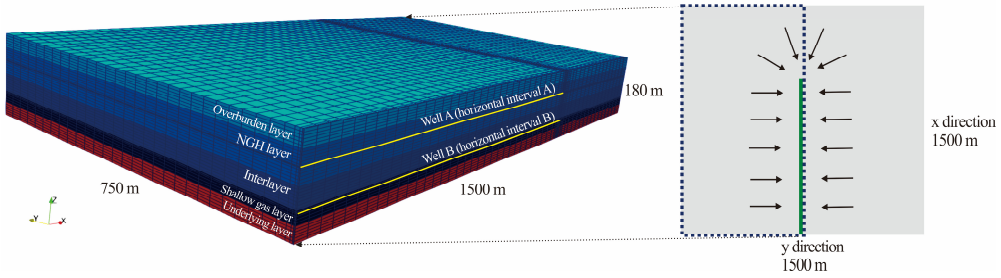

Figure 2. Schematic of conceptual geological system of the NGH layer and shallow gas layer in the target area.

2.3. Well Design and Production Schemes

Two horizontal wells are set in NGHs and shallow gas layers, respectively. As shown in Figure 2, the horizontal interval A is located in the middle of the NGHs layer, having a length of 1000 m. In the production of traditional gas reservoirs, to avoid or delay the incursion of the water in the underlying layer, the perforation is always placed at the top or upper interval of the gas layer; thus, the horizontal interval B is located 2 m below the top of the shallow gas layer, and the horizontal interval B is also 1000 m.

The gas production from horizontal interval 1 is applied with constant bottom hole pressure at 5 MPa, to obtain the dissociation of NGHs as much as possible. The gas production from horizontal interval 2 is applied with a constant production rate at 1×10^6 m^3/day, relying on the daily production rates for common gas reservoirs, until the bottom hole pressure is reduced to 5 MPa (Co-P(5.0) in Table 1). To illuminate the improvement in the efficiency of co-production, two single production cases for NGHs alone and shallow gas alone were calculated as comparisons (NGHs-P(5.0) and SGa-P(5.0) in Table 1). Besides, other critical factors influencing the production behaviors, such as the production pressure (Co-P(3.0) and Co-P(7.0)) and the length of horizontal intervals (Co-L(330), Co-L(660) and Co-L(1330)), were also analyzed; the details are exhibited in Table 1.

Table 1. Summary of production modes, bottom hole pressure and well lengths of each case.

Cases	Production Mode	Production Pressure/MPa	Length of Interval A/m	Length of Interval B/m	Description
Co-P(5.0)	NGHs + SG [a]	5.0	1000	1000	Base case for co-production.
NGHs-P(5.0)	NGHs	5.0	1000	-	Single production for NGHs.
SG [a]-P(5.0)	SG [a]	-	-	1000	Single production for shallow gas.
Co-P(3.0)	NGHs + SG [a]	3.0	1000	1000	Co-production with BHP [b] at 3.0 MPa.
Co-P(7.0)	NGHs + SG [a]	7.0	1000	1000	Co-production with BHP [b] at 7.0 MPa.
Co-L(330)	NGHs + SG [a]	5.0	330	330	Co-production with two 330 m horizontal intervals.
Co-L(660)	NGHs + SG [a]	5.0	660	660	Co-production with two 660 m horizontal intervals.
Co-L(1330)	NGHs + SG [a]	5.0	1330	1330	Co-production with two 1330 m horizontal intervals.

[a] SG represents shallow gas. [b] BHP represents bottom hole pressure.

2.4. Properties of the Reservoirs

Based on the homogeneous assumption, all the physical and thermal-dynamic properties within the same material are consistent. According to the logging data, the porosity of the NGHs and shallow gas layers are set as 0.45 and 0.26. The permeability of the NGHs and shallow gas layers are 20 mD and 200 mD. The hydrate and water saturation in the NGHs are 40% and 60%, respectively. The gas and water saturations in the shallow gas layer are 87% and 13%. To simulate the gas extraction from shallow gas reservoirs, the migration of the water phase should be strictly constricted. Therefore, the irreducible water saturation is set at 13%, to ensure the mobility of gas flow in the gas layer. The grids of the two horizontal wells have a porosity of 1.0, and a permeability of 1.0×10^{-9} m^2. Other parameters listed in Table 2 are sourced from Zhao et al. [28], Jin et al. [29], and Cheng et al. [27].

Table 2. Thermal-physical properties and initial conditions in simulations.

Parameters	Values Utilized in NGHs Layer	Values Utilized in Shallow Gas Layer	Values Utilized in Overburden/ Underlying Layers	Values Utilized in Interlayer
Density/kg/m^3	2.65×10^3	2.60×10^3	2.65×10^3	2.65×10^3
Porosity/unitless	0.45	0.26	0.02	0.02
Permeability/m^2	2.0×10^{-15}	2.0×10^{-13}	2.0×10^{-17}	2.0×10^{-17}
Phase characteristics	AqH	AqG	Aqu	Aqu
Water saturation/unitless	0.6	0.13	1.0	1.0
Hydrate Saturation/unitless	0.4	-	-	-
Gas saturation/unitless	-	0.87	-	-
Formation heat conductivity under fully saturated conditions W/m/°C	1.0			
Formation heat conductivity under desaturated conditions W/m/°C	3.1			
Rock grain specific heat J/kg/°C	1.0×10^3			
Pore compressibility/Pa^{-1}	1.0×10^{-8}			
Irreducible water saturation/unitless	0.35	0.13	0.35	0.35
Irreducible gas saturation/unitless	0.02	0.02	0.02	0.02
Permeability exponential for aquifer/unitless	3.572			
Permeability exponential for gas phase/unitless	2.0	2.0	3.572	3.572

2.5. The Initial and Boundary Conditions

In this work, the pressure gradient was calculated based on the acceleration of gravity in the QDNB and the density of the movable phases. Apart from the shallow gas layers, the movable phase in the other four layers was aquifer; thus, the hydrostatic pressure was utilized. For the shallow gas layer, the reservoir pressure was calculated based on the density of methane, the acceleration of gravity in the QDNB, and water depth. In particular, at the base of the NGHs layer, the reservoir pressure and temperature were 20.09 MPa and 17.21 °C, in layers deeper than which the pressure and temperature dissatisfy the phase-equilibrium conditions for NGHs. The pore fluids in the NGHs layer consisted of hydrate and aquifer; the hydrate saturation was 40% and the water saturation was 60%. The pore fluids in the shallow gas layer consisted of free gas and irreducible water; the gas saturation was 87% and the water saturation was 13%. The pore fluids in the overburden layer, interlayer and underlying layer are aquifer. The initial porosity and permeability in different layers are listed in Table 2. Two thin planes with a thickness of 0.01 m are assigned at the top and the bottom of the model, where the pressure, temperature and other properties are constant during the whole co-production processes. The pressure, temperature, hydrate saturation and gas saturation fields at the x-z plane are shown in Figure 3.

The reservoir pressure and temperature increase with depth (Figure 3a,b), and the ranges of pressure and temperature were consistent with geological data. The NGHs only occurred in the NGHs layer, with hydrate saturation (S_{hyd}) equaling 40% (Figure 3c). The natural gas only occurred in the shallow gas layer, with gas saturation (S_{gas}) equaling 40% (Figure 3d).

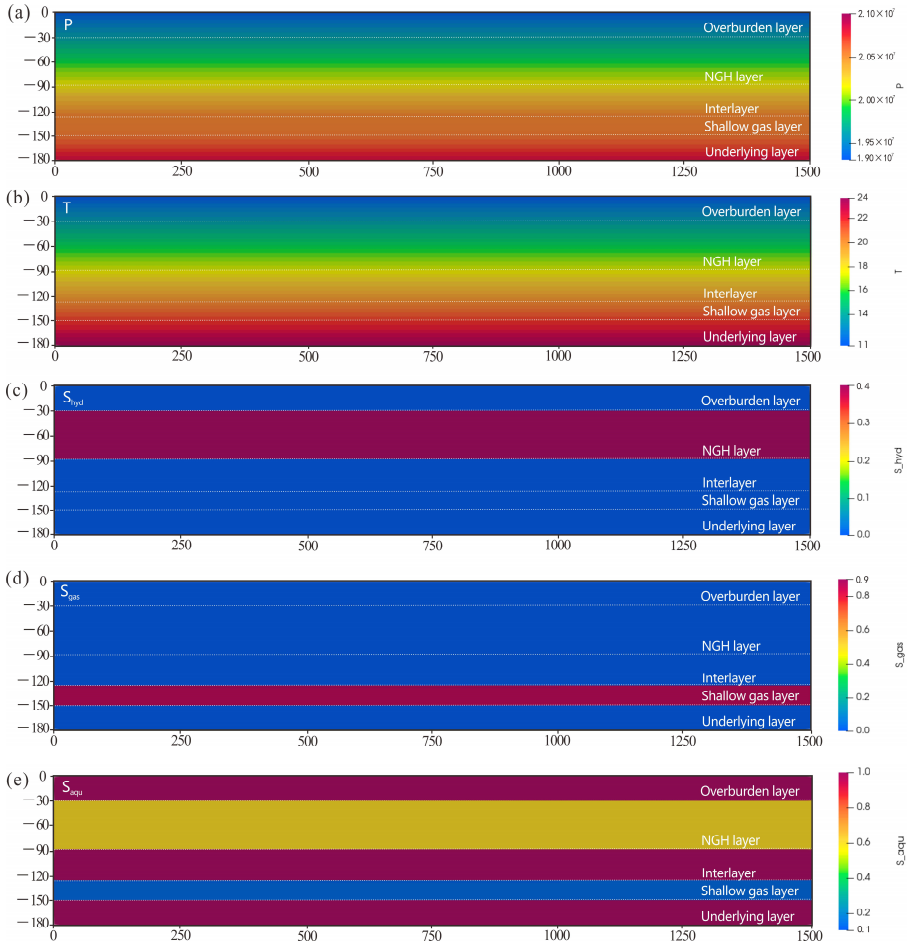

Figure 3. Pressure (**a**), temperature (**b**), hydrate saturation (**c**), gas saturation (**d**) and water saturation (**e**) distribution fields of the NGHs and shallow gas reservoirs at the initial state.

3. Results

3.1. The Improvements in Gas Yields from Separate Wells Through Co-Production with Shallow Gas

The daily gas production rates for co-production of NGHs and shallow gas reservoirs (case: Co-P(5.0)) and producing NGHs alone (case: NGHs-P(5.0)) are shown in Figure 4a with separate production rates obtained from horizontal interval A and B (well A/B). Well A was arranged in the NGHs layer, represented by blue curves, while well B was arranged in the shallow gas layer, represented by green curves. As shown in Figure 4a, the production rates from well B in case Co-P(5.0) remained approximately 1.08 million m^3 per day for ~2500 days until the flow bottom hole pressure reduced to 5.0 MPa, and immediately decayed to a low level. For cases Co-P(5.0) and NGHs-P(5.0), the gas production rates obtained from well A were the same as each other during 0 to ~760 days, both experiencing a fluctuating phase (until ~180 days), then increasing to 1×10^4 m^3 per day. After 760 days, the gas production rate in Co-P(5.0) stabilized at ~1×10^4 m^3 per day, while for NGHs-P(5.0), the gas production rate increased with time and plotted 5.23×10^4 m^3 per day at the end of the 10th year, which was ~5.0 times that obtained from co-production.

The cumulative gas productions obtained from the co-production, NGHs production alone and shallow gas production alone are displayed in Figure 4b. The cumulative production rates in co-production and shallow gas production situations were enormous compared with that in NGHs production, both exhibiting rapid growth trends during 0 to ~2500 days. The rapid growth was attributed to the stabilized production of well B

in the shallow gas layer. When the bottom hole pressure of well B depleted to 5.0 MPa, the production rates decreased correspondingly; thus, the growth trends of accumulated gas production slowed down immediately after ~2500 days. The cumulative production rates from well A in the situation of producing NGHs alone increased with time during the whole cycle, corresponding to the increasing trend in the daily production rate of NGHs (Figure 4a). To figure out the precise contributions of the output from well A, the cumulative gas yields from well A and B in Co-P(5.0) were analyzed in Figure 4b. The percentage of gas volume produced from well A (blue curve) in co-production showed an upward trend and plotted below 1.25% in the 10th year, indicating the dominate role of shallow gas in achieving superior cumulative gas yields.

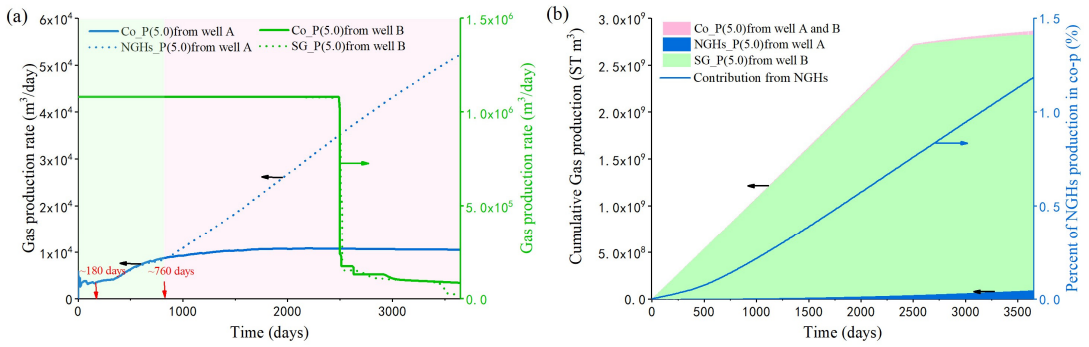

Figure 4. The daily gas production rate (**a**) and cumulative gas production rate (**b**) from separate wells for the co-production of NGHs and shallow gas (case: Co-P(5.0)), production of NGHs alone (case: NGHs-P(5.0)) and production of shallow gas alone (case: SG-P(5.0)) over 10 years. Arrows pointing to the left indicates the primary y-axis on the left side, arrows pointing to the right indicates the secondary y-axis on the right side. The green and pink background color in (**a**) represents consistent trend of change for Co_P(5.0) and NGHs_P(5.0) from well A.

To investigate well output in co-production and separate production, the gas production rates of co-production and producing NGHs/shallow gas alone were analyzed. In the situation of Co-P(5.0), the summation of cumulative gas production from well B (shallow gas layer) and well A (NGHs layer) surpassed 2.863 $\times$ 10^9 m^3 in the 10th year, among which 2.829 $\times$ 10^9 m^3 was obtained from well B and 3.391 $\times$ 10^7 m^3 from well A. The cumulative gas production in case SG-P(5.0) was 2.822 $\times$ 10^9 m^3, lower than that obtained from co-production (2.829 $\times$ 10^9 m^3). However, the cumulative gas production in case NGHs-P(5.0) was 9.120 $\times$ 10^7 m^3, which was 2.7 times that obtained from well B in Co-P(5.0) (3.391 $\times$ 10^7 m^3). The summation of the cumulative gas production of NGHs alone and SG alone was 2.913 $\times$ 10^9 m^3, which was 1.75% greater than the gas yields obtained from the co-production. However, this does not imply that the output from the combined exploitation of NGHs and shallow gas is inferior to the sum of the individual productions of these two types of resources. In this model, the interlayer is permeable; thus, the gas yields for well A during the standalone exploitation of NGHs actually contains the natural gas migrating from the lower shallow gas layer. Simply summing up the individual production results of the two types of resources leads to the double-counting of the migrated shallow gas, thereby creating the erroneous impression that the combined gas production is lower than the sum of the productions of the two resources.

In summary, with the involvement of the extraction from shallow gas, the overall gas production rates are improved by approximately 25~50 times, satisfying the criteria for commercial production.

3.2. The Enhancement for NGHs Dissociation in Co-Production with Shallow Gas

3.2.1. The Improvements in Gas Volume Released from the Dissociation of NGHs

Due to complex fluid migration in reservoirs, the gas produced from the well in the NGH layer does not represent the gas released from the dissociation of NGHs. Therefore, the dissociation of NGHs was analyzed in this section. As shown in Figure 5a, the volume rates of CH_4 released from the dissociation of NGHs in co-production and NGHs production are represented by pink and jade dots. In the situation of producing NGHs alone, the daily volume rate increased to ~7600 m^3/day rapidly at 0 to ~120 days and stabilized at ~9800 m^3/day until the ~690th day; the cumulative gas production was 3.66 × 10^7 m^3 during the whole simulated cycle. In co-production, the daily volume rate of NGHs dissociation CH_4 also experienced a rapid growth at 0 to ~120 days, with a higher increase rate than that in the situation of producing NGHs alone, then jumped to 14,500 m^3/day at day ~505 and increased until around the 2250th day. On the ~2250th day, the volume rate of NGHs dissociation gas surpassed ~34,000 m^3/day, then decreased until the end of the simulation cycle. At the end of the 10th year, the cumulative volume of CH_4 induced by the dissociation of NGHs in Co_P(5.0) cases was approximately 8.96 × 10^7 m^3. In summary, compared with the situation of producing NGHs alone, the co-production enhanced the dissociation of NGHs in reservoirs, improving the peak volume rate and cumulative volume rate of CH_4 to 3.52 and 1.45 times.

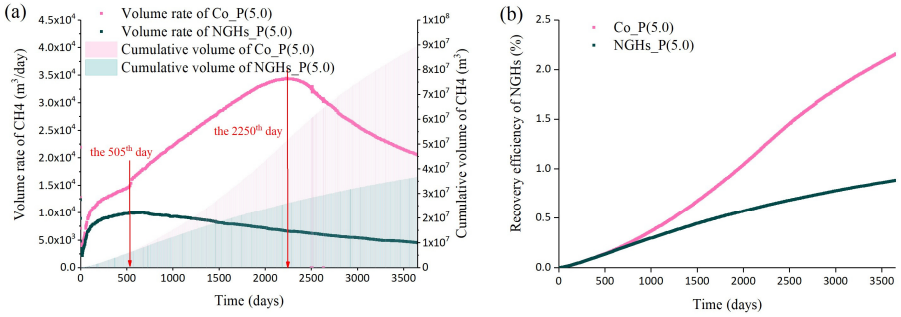

Figure 5. Volume rates (**a**) and recovery efficiency (**b**) of CH_4 obtained from the dissociation of NGHs.

Enhanced gas liberation through NGHs dissociation correlates with reduced residual hydrate saturation in reservoirs, thereby improving the overall recovery efficiency of NGHs. Figure 5b illustrates the comparative recovery efficiencies of standalone NGHs production versus co-production over the simulation period. Both scenarios demonstrate progressive enhancement in NGH recovery efficiency over time. By the end of the 10th year, the cumulative recovery efficiency reached approximately 0.9% for standalone production and 2.2% for co-production systems. This equates to a 2.4-fold improvement in NGH recovery efficiency attributable to synergistic co-production with shallow gas, highlighting the operational advantages of integrated resource recovery strategies.

3.2.2. The Enlargement in the Dissociation of NGHs near Wellbore Region and the Bottom of NGHs Layer

According to the volume rates of the CH_4 released from NGHs (Figure 5a), there were some critical points in the co-production: a rapid increase on the ~505th day; the peak volume rate on the 2250th day and the terminate state in the 10th year. To investigate the reasons for gas production behaviors from NGHs at these three points, the distribution fields of hydrate saturation alone and the horizontal interval (in x-z plane) in co-production and NGHs production are analyzed firstly (Figure 6). From an intuitive perspective, the hydrate saturation profiles exhibited consistency between co-production and NGHs production scenarios across the three simulated time intervals. Hydrate dissociation,

visually represented by blue regions in the color scale, first emerged in the wellbore and adjacent near-wellbore regions (Figure 6a,b). Over time, this dissociation zone expanded bidirectionally: radically propagating along the horizontal wellbore intervals and affecting NGH deposits beneath well A. On approximately the 2250th day, the dissociation fronts of NGHs migrated from near-wellbore areas into deeper reservoir strata (Figure 6c,d). Notably, hydrate saturation beneath well A exhibited a significant decline. In the 10th year, the hydrate dissociation region at near-wellbore areas expanded furthermore, and the hydrate saturation of the reservoir beneath well A experienced a pronounced reduction (Figure 6e,f).

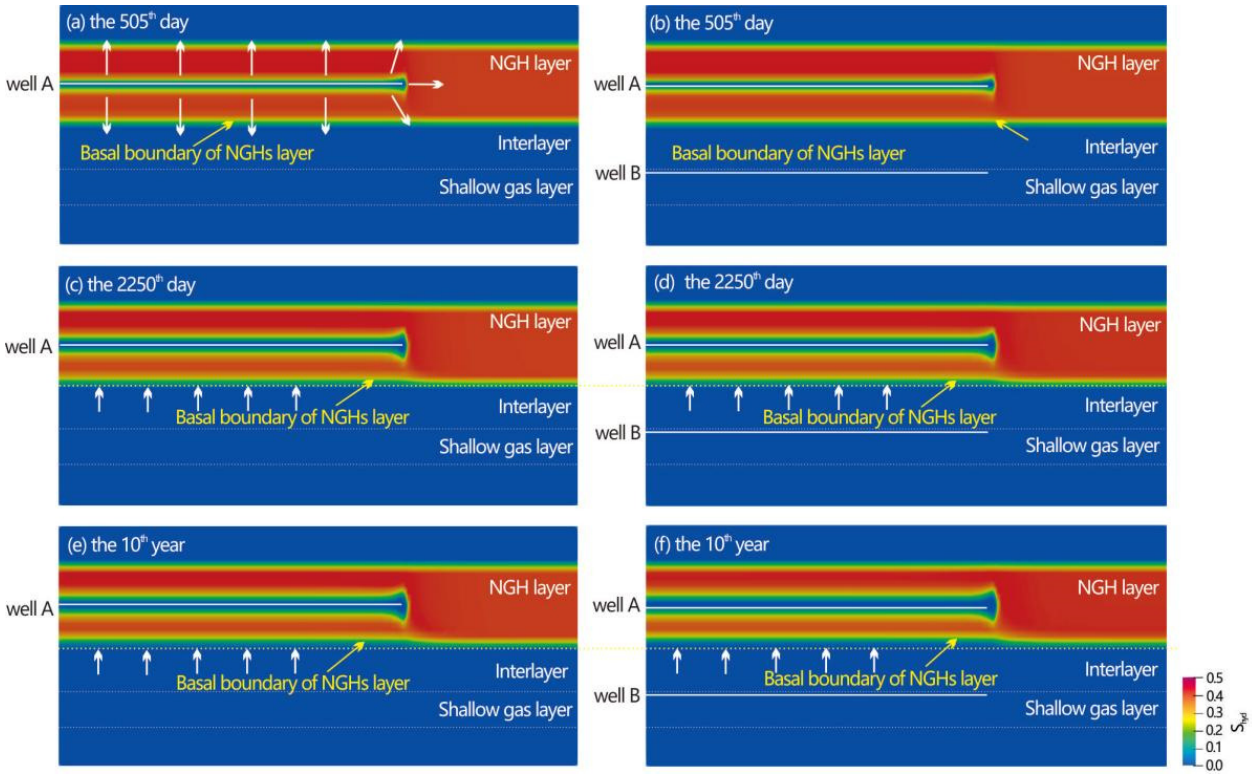

Figure 6. Hydrate saturation fields for NGHs production and co-production of NGHs and shallow gas at critical simulated time intervals. (**a**,**c**,**e**) = NGHs production only and (**b**,**d**,**f**) = co-production.

To quantitatively assess the influence of co-production strategies on NGH dissociation dynamics, we determined the residual hydrate volumes under two distinct production scenarios (co-production and NGHs production). The residual hydrate volume was defined as the ratio of hydrate volume retained within pores at simulated time nodes to the initial hydrate volume before production, and the depth-dependent distributions of the residual hydrate volume are presented in Figure 7. On the 505th day, 2250th day and 10th year, the residual volume of hydrates in the two production scenarios exhibited consistency. Specifically, minimal residual volumes were observed at approximately 60 m below the seafloor (mbsf); meanwhile, a progressive decrease was noted at the basal boundary. On the 505th day, comparable residual hydrate volumes were observed in both production scenarios. However, on the 2250th day, a distinct reduction in residual volumes of hydrate occurred within the NGHs layer under co-production conditions, with this disparity further intensifying after 10 years of production. This progressive divergence in residual volumes between the two strategies verified the enhancement in dissociation efficiency of NGHs when implementing co-production techniques.

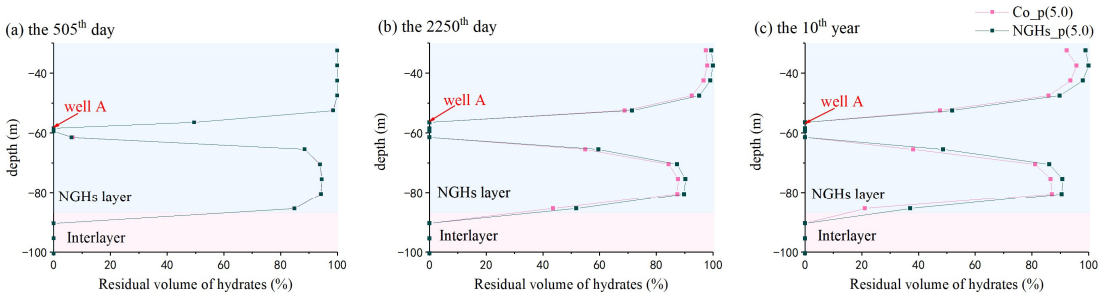

Figure 7. Depth-dependent distributions of residual hydrate volume in the two production scenarios (pink dots represent co-production, and jade dots represent NGHs production) on the 505th day (**a**), the 2250th day (**b**) and the 10th year (**c**). Blue and pink background color represent for NGHs layer and interlayer, respectively.

To analyze the reasons for the dissociation of NGHs, the pressure fields on the ~505th, 2250th, and 3600th days are displayed in Figure 8. In the situations of NGHs production, the pressure drop propagated from well A into the NGHs reservoir with time; ultimately, the pressure at the basal boundary of the NGHs layer depleted to approximately 11.86~12.74 MPa by the 10th year (Figures 8e and 9c). In the co-production scenario, the pressure drop in the shallow gas layer created a contiguous pressure depletion zone with well A. The pressure of the reservoir from well A to the interlayer was significantly lower than that observed in standalone NGHs production during the same period (Figure 8a,b on the 505th day; Figure 8c,d on the 2250th day; Figure 8e,f in the 10th year). A quantitative analysis of these differences is presented in Figure 9. On the 505th day (Figure 9a), the pressure in the NGHs layer was identical in both production scenarios, whereas when shallow gas was produced alongside NGHs, the pressure in the interlayer was lower than that in NGHs production. On the 2250th day (Figure 9b), the pressure in the NGHs layer in co-production was 0.56~2.06 MPa lower than that in NGHs production. Within the NGHs layer, the differences in the pressure in co-production and NGHs production increased with depth from well A to deeper reservoirs, and the maximum pressure difference occurred at the basal boundary of NGHs layer (2.06 MPa). The disparity in pressure induced by the two production strategies became more pronounced after 10 years of production, with pressure differences at the basal boundary exceeding 2.38 MPa (Figure 9c). In conclusion, co-production with the shallow gas reservoir enlarged the pressure drop region, particularly at the interlayer and basal boundary of the NGHs layer. The pressure drop of the interlayer led to a pressure reduction at the bottom of the NGHs layer, which provided a driving force for the dissociation of NGHs, probably resulting in jumps in the volume rate of CH_4 (Figure 5a), thereby enhancing the dissociation of hydrates at the bottom of the NGHs layer.

3.2.3. The Mismatches Between Well Output and CH_4 Released from NGHs Dissociation

The placement of well A within the NGHs layer is primarily aimed at extracting the natural gas resources in the NGHs. However, there was a significant discrepancy between the gas production rates obtained from well A (Figure 4a) and the volume rate of CH_4 induced by the dissociation of NGHs (Figure 5a), whether in the case of co-production or standalone production of NGHs. In the co-production scenario, the daily gas production from well A stabilized at ~1.07×10^4 m^3/day after ~760 days of production, whereas the daily dissociation volume of CH_4 from hydrate dissociation was ~3.4×10^4 m^3/day after ~2250 days of production, exhibiting different values and trends. By the end of the 10th year, the cumulative gas volume from well A and the volume from hydrate dissociation were 3.39×10^7 m^3 and 8.96×10^7 m^3, implying that nearly 62.17% of gas released from hydrate dissociation was trapped in reservoir pores in an immobilized state. On the contrary, there

were totally different results in the standalone NGHs production scenario, where the peak daily gas production rates from well A and dissociated gas volume from NGHs were ~5.23 $\times 10^4$ m^3 and ~9800 m^3, implying that the gas in shallow gas reservoirs migrated into the NGHs layer and was produced from well A.

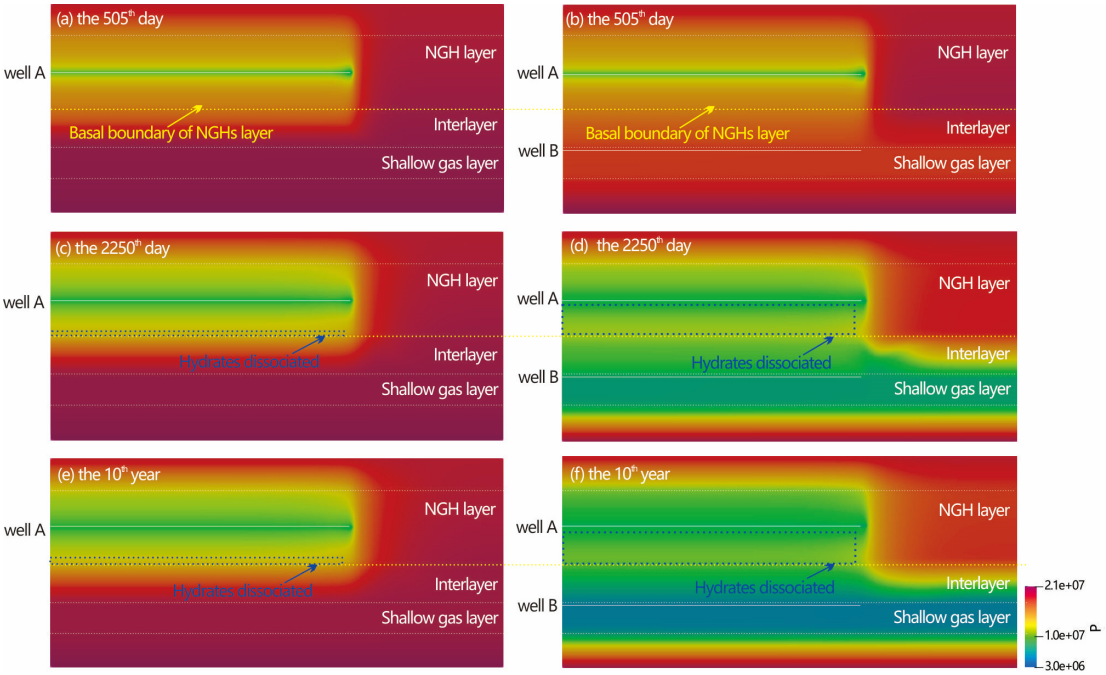

Figure 8. Distribution fields of pressure for NGHs production and co-production of NGHs and shallow gas at critical simulated time intervals. (**a**,**c**,**e**) = NGHs production only and (**b**,**d**,**f**) = co-production.

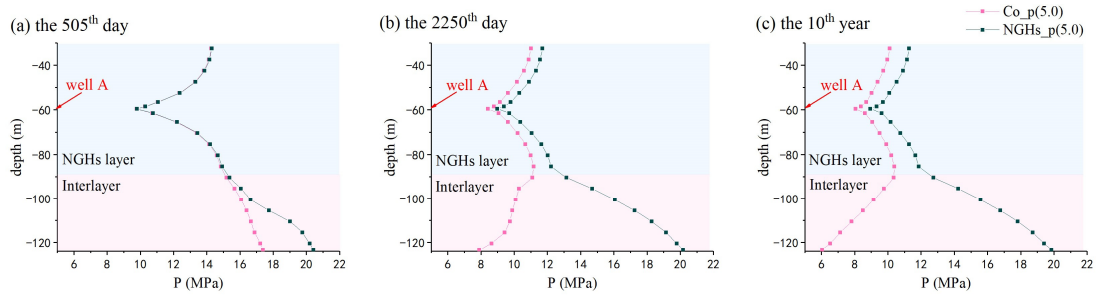

Figure 9. Reservoir pressure distribution with depth on the 505th day (**a**), the 2250th day (**b**) and the 10th year (**c**). Blue and pink background color represent for NGHs layer and interlayer, respectively.

To verify these two hypotheses of gas migration in the NGHs layer and between layers, a case in which the amounts of dissociated gas trapped in pores were adjusted by setting irreducible gas saturation to 0 in the NGHs layer, and a case in which the interlayer migration was controlled by setting an impermeable interlayer were simulated in this section. When irreducible gas saturation was set to 0, the peak daily production of well A increased by 26.31%, rising from approximately 1.07 $\times$ 10^4 to 1.35 $\times$ 10^4 m^3/day (Figure 10a). In contrast, the volume rate of CH_4 released from NGHs dissociation decreased from ~34,000 to ~30,000 m^3/day. Notably, a persistent discrepancy existed between the dissociated gas volume (~3.0 $\times$ 10^4 m^3/day) and the total output of well A (~1.35 $\times$ 10^4 m^3/day), suggesting complex flow mechanisms in the NGHs layer that warrant further investigation. In the other case, the presence of an impermeable interlayer separating the NGHs and the shallow gas layer resulted in a significant decline in production rates from well A, decreasing from 5.23 $\times$ 10^4 to 9904 m^3/day (Figure 10b). This reduction verified that

despite the shallow gas layer not being actively produced, the gas in the shallow gas layer could migrate upward and be produced from well A. Low permeable interlayers effectively mitigate the upward migration of gas from the underlying shallow reservoir and alleviate interference between layers.

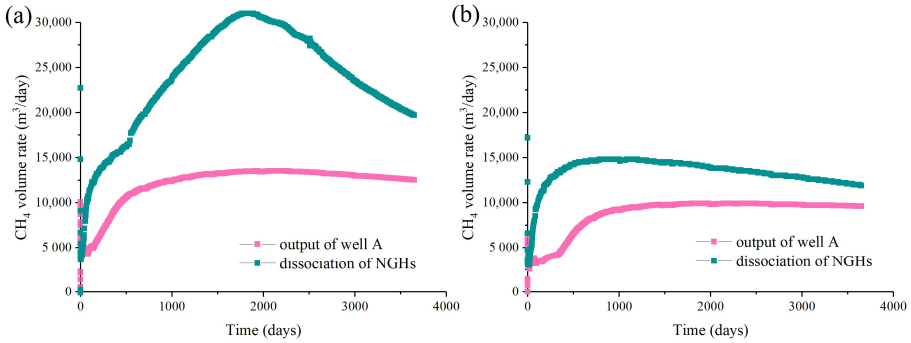

Figure 10. Comparisons between output of well A and CH_4 volume released from NGHs dissociation in co-production with irreducible gas saturation in NGH layer equals 0 (**a**), and NGHs standalone production with impermeable interlayer (**b**).

3.3. Sensitivity Analysis with a Focus on the Impact of Key Factors in Production

The daily and accumulative production rate from well A and B under production pressures of 3.0, 5.0, and 7.0 MPa are depicted in Figure 11. For well A (arranged in the NGH layer), a lower production pressure significantly enhanced the daily gas production rates. Specifically, at a production pressure of 3.0 MPa, the peak daily production exceeded 15,000 m^3, reflecting a 50% increase compared to the base case at 5.0 MPa. The cumulative production rate by the end of the 10th year plotted at 4.82×10^7, 3.39×10^7 and 2.26×10^7 ST m^3 under production pressures of 3.0, 5.0 and 7.0 MPa, respectively. At a production pressure of 3.0 MPa, the cumulative production exceeded a 42% increase compared to the base case. For well B (located in the shallow gas layer), which had been producing at a constant rate until the reservoir pressure dropped to the production pressure of well A, the daily and cumulative gas outputs remained consistent across Co-P(3.0), Co-P(5.0) and Co-P(7.0) scenarios before the bottom hole pressure of well B decreased to the production pressure of well A. Upon reaching this pressure threshold, the daily gas production of well B dropped below 2.5×10^5 m^3, and the growth rate of cumulative gas production slowed down. By the end of the 10th year, the cumulative gas production from well B amounted to 2.92×10^9, 2.83×10^9 and 2.68×10^9 m^3 across Co-P(3.0), Co-P(5.0) and Co-P(7.0) scenarios, and a 3.2% increase in production was observed at a production pressure of 3.0 MPa.

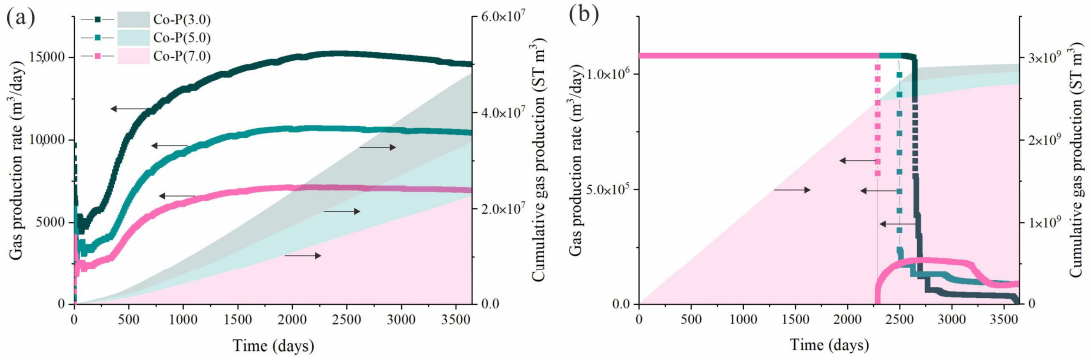

Figure 11. The daily and cumulative gas production rates from well A (**a**) and well B (**b**) in cases with different production pressures over 10 years. Arrows pointing to the left indicates the primary y-axis on the left side, arrows pointing to the right indicates the secondary y-axis on the right side.

The daily and cumulative gas production rates from well A and B, with lengths of the horizontal interval of 330 m, 660 m, 1000 m, 1330 m, are illustrated in Figure 12. For well A, the gas production rates were influenced by the length of the horizontal interval. The daily gas production rates at steady phase and cumulative gas production rates were 3514, 6946, 10,433, 13,873 m^3/day and 1.15 × 10^7, 2.26 × 10^7, 3.39 × 10^7, 4.50 × 10^7 ST m^3 for horizontal lengths of 330, 660, 1000 and 1330 m. This indicated that the gas production from wells in the NGH layer is substantially proportional to the horizontal length. In contrast, for well B, no clear pattern in daily or cumulative gas production was observed across different lengths. Consequently, the well length influences the production from wells in the NGH layers, but it does not affect production in shallow gas layers with satisfied permeability.

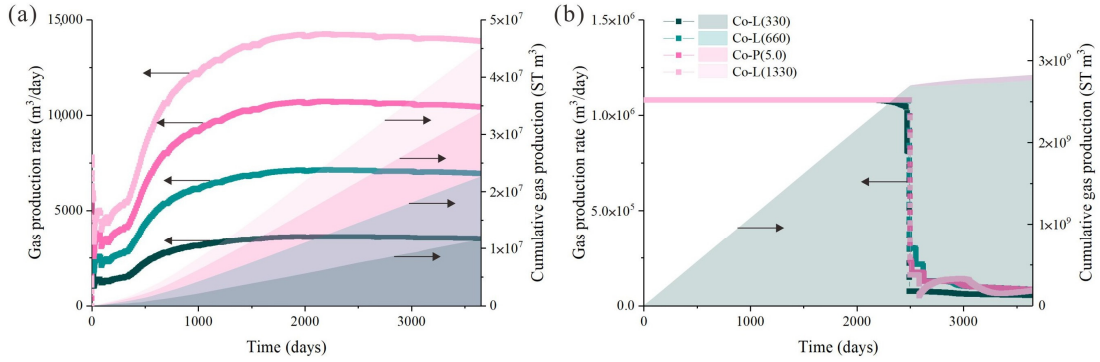

Figure 12. The daily and cumulative gas production rates from well A (**a**) and well B (**b**) in cases with different lengths of horizontal intervals over 10 years. Arrows pointing to the left indicates the primary y-axis on the left side, arrows pointing to the right indicates the secondary y-axis on the right side.

3.4. Optimized Well Pattern

In this work, due to the inherent low permeability characteristics observed in NGH layers, the propagation of pressure within these formations is notably constrained, as visually depicted in Figure 6. This limited pressure transmission significantly impedes the natural or induced dissociative processes essential for gas extraction, thereby necessitating innovative strategies to enhance reservoir contact and improve recovery efficiency. In response to this challenge, the implementation of horizontal well patterns emerges as a promising solution, designed to expand the spatial extent of NGH dissociation by maximizing the interaction surface between the wellbore and the reservoir matrix. This approach aims to overcome the intrinsic limitations imposed by the reservoir's low permeability, facilitating a more uniform and effective pressure distribution, and ultimately enhancing gas production rates. Conversely, in scenarios where the overlying gas layers exhibit satisfactory permeability, the conventional approach of employing a vertical well configuration, coupled with perforation intervals positioned near the upper reaches of the shallow gas zone, proved sufficient for effective gas production. This type of well design capitalizes on the higher permeability pathways available, allowing for efficient gas migration towards the wellbore with minimal need for extensive reservoir stimulation or complex well architectures.

In order to take into account factors such as construction techniques and cost expenditure while achieving the highest possible gas production from the NGH layer and shallow gas layer, it is recommended to drill a vertical well that penetrates the gas hydrate layer to reach the shallow gas layer, and establish horizontal well branches within the gas hydrate layer and perform full-segment perforation. In the shallow gas layer, it is recommended to conduct scalp-adjacent (i.e., extremely close to the top of the targeted zone) perforation at the top of the gas layer in the main vertical well, as illustrated in Figure 13.

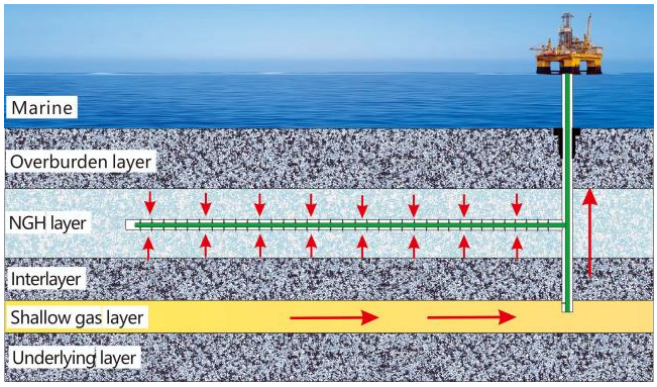

Figure 13. Recommended well pattern for the co-production of NGH layer and shallow gas layer.

4. Discussion

4.1. Validity and Relevance of Outcomes

Here, a 3D model of the Lingshui X field has been developed, incorporating key reservoir characteristics: it spans an area of 1.5 × 1.5 km, boasts total hydrate resources of 2.35 × 10^7 m^3, contains 1.22 × 10^7 m^3 of free methane gas, and holds a total of 5.0 × 10^9 kg methane in the model, all of which align with the actual field reserve magnitudes. Over a 10-year co-production period, the cumulative gas outputs from well A and B were 1.5 × 10^7 m^3 and 2.829 × 10^9 m^3, respectively. Furthermore, the dissociation of NGHs was significantly enhanced through the use of dual horizontal well systems, which facilitated concurrent shallow gas extraction. To validate the results presented in this work, a comparative analysis of co-production simulations for NGHs and shallow/associated gas has been summarized (Table 3). Due to the varying simulation durations across different studies, the cumulative gas production from NGH layers and shallow gas reservoirs by the end of the 10th year was normalized using average gas yield rates (denoted by * in Table 3). From the perspective of the order of magnitude of accumulative gas production, Cheng et al. [26] reported that the cumulative gas yields were two orders of magnitude lower than those of other studies. For the remaining studies, the cumulative gas production ranges from 10^6 to 10^7 m^3 from NGH layers and 10^7 to 10^8 m^3 from shallow gas reservoirs. The cumulative production of NGHs and shallow gas from this study is 1.25 to 19.4 times and 12.9 to 1.77 × 10^5 times higher. Excluding the data from Cheng et al. [26] narrows these ranges to 1.25~6.25 times for NGHs and 12.9~257.2 times for shallow gas. Regarding the gas production volume from the NGH layer, the comparison suggests a satisfactory level of consistency across different cases. The three cases that utilized horizontal wells achieved gas production of 10^7 m^3 from the NGH layer, whereas the gas production from vertical wells was only on the order of 10^6 m^3, illuminating the improvement in gas production from the NGH layer achieved by horizontal wells. The gas produced from the shallow gas layer in this study is significantly higher, which is greatly influenced by well pattern, pressure and permeability in gas layers. As shown in Table 3, the highest accumulative gas production from shallow gas reservoirs was obtained in the case simulated in this study, which featured relatively higher reservoir pressure (approximately 20 MPa), ideal permeability (200 mD) and superior well patterns (horizontal wells). The three cases with low permeability in gas layer (6.8 to 7.4 mD) achieved a well output of 10^7 m^3 when applying a vertical well, while the well output improved to 10^8 m^3 when horizontal wells were employed. Most notably, when the permeability was increased to 200 mD, the gas production reached 10^9 m^3.

Table 3. Summary of numerical results for co-production of NGHs and shallow gas.

Sources	Accumulative Production of NGHs at 10th Year/m^3	Accumulative Production of Shallow Gas at 10th Year/m^3	Well Patterns/ Length of Perforation Interval of the Well in NGHs Layer and (+) Shallow Gas Layer	Initial Pressure of Gas Layer/MPa	Permeability of Gas Layer/mD
This study	1.5×10^7	2.829×10^9	Horizontal 1000 m + 1000 m	19~20	200
Zhao et al. [27]	~2.4×10^6 *	~1.5×10^7 *	Vertical 75.2 m + 30 m	17.48~18.19	7.4
Jin et al. [28]	~6.7×10^6 *	~2.2×10^8 *	Vertical 60 m + 12 m	17~18	6.8
Wei et al. [30]	~6.3×10^6 *	~1.1×10^7 *	Vertical 30 m + 16 m	14~15	7.4
Wei et al. [30]	~1.2×10^7 *	~2.3×10^7 *	Horizontal 50 m + 50 m	14~15	7.4
Cheng et al. [26]	~7.7×10^5 *	~1.6×10^5 *	Horizontal 300 m + 300 m	19~20	0.1

* represents estimated values.

4.2. Limitation and Further Research Directions

Two primary limitations exist in this study. Firstly, the grid configuration built in this study is incapable of accurately capturing the complex heterogeneity of actual reservoirs in the study area. Due to the limited availability of geophysical and geological data in the target area, a three-dimensional geological model was not obtained. Instead, a planar mechanistic numerical model with vertical heterogeneity was constructed by extending the logging data from a specific well location outward in horizontal directions. Consequently, the results of this study, including daily gas production rates and production duration, cannot be regarded as reliable references for actual field development. Secondly, owing to the absence of experimental results on relative permeability from core samples in the study area, the input parameters for the relative permeability module in TOUGH had to be determined based on empirical data. These parameters exert a certain influence on gas production patterns. Therefore, this study primarily focuses on analyzing the impact of other factors on gas production patterns under the condition of consistent empirical parameters in the relative permeability module.

In future research, on the one hand, a coarsened grid of the geological model—established based on seismic data and logging data from multiple wells—will be employed to investigate the integrated production of gas hydrates and shallow gas, with the objective of obtaining practically reliable co-production results. On the other hand, the incorporation of relative permeability from experimental core samples across different stratigraphic layers will enable the derivation of accurate and reliable gas production patterns.

5. Conclusions

Under the numerical simulation conditions of this study, the co-production with shallow gas through dual horizontal wells boosts the total gas production from natural gas hydrates and shallow gas systems to 25–50 times (compared to standalone NGHs extraction), reaching the rule-of-thumb for commercially viable production rates from offshore gas wells.

Co-production notably raises the gas volume released from the hydrate dissociation via horizontal wells to 2.4 times that of hydrate standalone production through a single horizontal well. In the co-production scenario, the volume of gas released from hydrate dissociation surged at approximately 505 days and peaked at approximately 2250 days. The reservoir pressure and hydrate saturation in the co-production scenario were observed to be lower than producing natural gas hydrates alone, and the hydrate bottom interface

moved up significantly during co-production, indicating the impacts of shallow gas on hydrate dissociation and gas production dynamics.

The fluid flow mechanism within the reservoir during the co-production of hydrates and shallow gas is extremely complex. Over 60% of the gas generated from hydrate dissociation was trapped within reservoir pores and could not be produced from the horizontal well in the hydrate-bearing layer. Even after increasing the saturation of irreducible gas, the gas production rates of the horizontal well in the hydrate-bearing layer barely rose by approximately 26%, with a significant amount of dissociated gas still unable to be produced from the wellbore.

The sensitivity analysis indicated that lower production pressures substantially boosted daily and cumulative gas output from the horizontal hydrate well. When the production pressure is reduced from 5 MPa to 3 MPa, the daily gas production rate increases by 50%, and the cumulative gas production increases by 42%; however, it has a minor impact on the gas production of the horizontal well in the shallow gas layer. Due to the low permeability of the hydrate layer, extending the length of the horizontal interval of the well in the hydrate-bearing layer proportionally increased the gas volume from hydrate dissociation, while having essentially no effect on the gas production from the shallow gas layer with higher permeability. Therefore, under the circumstance of the reservoir conditions in this study, a combination of a vertical well and a horizontal interval was recommended for the co-production of hydrates and shallow gas.

Author Contributions: X.L.: Writing—original draft, Methodology, W.P.: Conceptualization, Methodology, Q.F.: Writing and review, Supervision, Funding acquisition Y.M.: Writing and review, Y.G.: Investigation, L.L.: Methodology, Software, H.W.: Investigation. All authors have read and agreed to the published version of the manuscript.

Funding: This work was funded by the Science and Technology Project of CNOOC Research Institute, China (grant no. SHW-ZYZL-02; KJQZ-2024-2005); Director's fund of State Key Laboratory of Offshore Natural Gas Hydrates (2025) (grant no. KJQZ-2025-2004); National Key Research and Development Program of China (grant no. 2021YFC28000903-02).

Data Availability Statement: The data presented in this study are available on request from the corresponding authors. The data are not publicly available, owing to the funding institution's research data-security commitments.

Acknowledgments: Special thanks to Weixin Pang for initiating this research with bold ideas and sustaining it with unwavering guidance; to Qiang Fu for empowering our work with essential platform support and insightful advice; to Yuhua Ma for perfecting our manuscript with scholarly rigor; to Lu Liu for turning technical roadblocks into stepping stones; and to Yang Ge and Huiyun Wen for enhancing our study with critical resources.

Conflicts of Interest: Authors Xin Lei, Weixin Pang, Qiang Fu, Yuhua Ma, Yang Ge, Huiyun Wen were employed by the Research Institute of China National Offshore Oil Corporation. The authors declare that the research was conducted in the absence of any commercial or financial relationships that could be construed as a potential conflict of interest.

References

1. Li, Z.; Fang, R.; Feng, L. Analysis of China's oil and gas imports and exports over the past 30 years. *Nat. Gas. Oil* **2025**, *43*, 136–143.
2. Ilyushin, Y.; Afanaseva, O. Development of a spatial-distributed control system for preparation of pulse gas. In Proceedings of the SGEM International Multidisciplinary Scientific GeoConference EXPO, Albena, Bulgaria, 18–24 August 2020; Volume 2, p. S08.061. [CrossRef]
3. Sloan, E. Fundamental principles and applications of natural gas hydrates. *Nature* **2003**, *426*, 353–359. [CrossRef]
4. Kleinberg, R.; Flaum, C.; Griffin, D.; Brewer, P.; Malby, G.; Peltzer, E.; Yesinowski, J. Deep sea NMR: Methane hydrate growth habit in porous media and its relationship to hydraulic permeability, deposit accumulation, and submarine slope stability. *J. Geophys. Res.* **2003**, *108*, 2508. [CrossRef]

5. Boswell, R.; Collett, T. Current perspectives on gas hydrate resources. *Energy Environ. Sci.* **2011**, *4*, 1206–1215. [CrossRef]
6. Moridis, G.; Collett, T.; Boswell, R.; Kurihara, M.; Reagan, M.; Koh, C.; Sloan, E. Toward production from gas hydrates: Current status, assessment of resources, and simulation-based evaluation of technology and potential. *SPE Reserv. Eval. Eng.* **2009**, *12*, 745–771. [CrossRef]
7. Qin, X.; Lu, C.; Wang, P.; Liang, Q. Hydrate phase transition and seepage mechanism during natural gas hydrate production tests in the South China Sea: A review and prospect. *Geol. China* **2022**, *49*, 749–769. (In Chinese with English abstract) [CrossRef]
8. Pang, X.; Hu, T.; Pu, T.; Xu, Z.; Wang, E.; Wang, W.; Li, C.; Zhang, X.; Liu, X.; Wu, Z.; et al. Risks and challenges of the industrial development of methane hydrate resources in the South ChinaSea. *Acta Pet. Sin.* **2024**, *45*, 1044–1060.
9. Zhu, W.; Huang, B.; Mi, L.; Wilkins, R.; Fu, N.; Xiao, X. Geochemistry, origin, and deep-water exploration potential of natural gases in the Pearl River Mouth and Qiongdongnan basins, South China Sea. *AAPG Bull.* **2009**, *93*, 741–761. [CrossRef]
10. Yu, X.; Wang, J.; Liang, J.; Li, S.; Zeng, X.; Li, W. Depositional characteristics and accumulation model of gas hydrates in northern South China Sea. *Mar. Pet. Geol.* **2014**, *56*, 74–86. [CrossRef]
11. Sun, J.; Zhang, L.; Ning, F.; Lei, H.; Liu, T.; Hu, G.; Lu, H.; Lu, J.; Liu, C.; Jiang, G.; et al. Production potential and stability of hydrate-bearing sediments at the site GMGS3-W19 in the South China Sea: A preliminary feasibility study. *Mar. Pet. Geol.* **2017**, *86*, 447–473. [CrossRef]
12. Wei, J.; Fang, Y.; Lu, H.; Lu, H.; Lu, J.; Liang, J.; Yang, S. Distribution and characteristics of natural gas hydrates in the Shenhu Sea Area, South China Sea. *Mar. Pet. Geol.* **2018**, *98*, 622–628. [CrossRef]
13. Kuang, Y.; Yang, L.; Li, Q.; Lv, X.; Li, Y.; Yu, B.; Leng, S.; Song, Y.; Zhao, J. Physical characteristic analysis of unconsolidated sediments containing gas hydrate recovered from the Shenhu Area of the South China sea. *J. Pet. Sci. Eng.* **2019**, *181*, 106173. [CrossRef]
14. Zhang, W.; Liang, J.; Wei, J.; Lu, J.; Su, P.; Lin, L.; Huang, W.; Guo, Y.; Deng, W.; Yang, X.; et al. Geological and geophysical features of and controls on occurrence and accumulation of gas hydrates in the first offshore gas-hydrate production test region in the Shenhu area, Northern South China Sea. *Mar. Pet. Geol.* **2020**, *114*, 104191. [CrossRef]
15. Qin, X.; Lu, J.; Lu, H.; Qiu, H.; Liang, J.; Kang, D.; Zhan, L.; Lu, H.; Kuang, Z. Coexistence of natural gas hydrate, free gas and water in the gas hydrate system in the Shenhu Area, South China Sea. *China Geol.* **2020**, *3*, 210–220. [CrossRef]
16. Lei, X.; Yao, Y.; Qin, X.; Lu, C.; Luo, W.; Wen, Z.; Yuan, X. Pore structure changes induced by hydrate dissociation: An example of the unconsolidated clayey-silty hydrate bearing sediment reservoir in the South China Sea. *Mar. Geol.* **2022**, *443*, 106689. [CrossRef]
17. Ye, J.; Qin, X.; Xie, W.; Lu, H.; Ma, B.; Qiu, H.; Liang, J.; Lu, J.; Kuang, Z.; Lu, C.; et al. Main progress of the second gas hydrate trial production in the South China Sea. *Geol. China* **2020**, *47*, 557–568.
18. Ye, J.; Qin, X.; Xie, W.; Lu, H.; Ma, B.; Qiu, H.; Liang, J.; Lu, J.; Kuang, Z.; Lu, C.; et al. The second natural gas hydrate production test in the South China Sea. *China Geol.* **2020**, *3*, 197–209. [CrossRef]
19. Hancock, S.; Collett, T.; Dallimore, S.; Satoh, T.; Inoue, T.; Huenges, E.; Henninges, J.; Weatherill, B. Overview of thermal-stimulation production-test results for the JAPEX/JNOC/GSC Mallik 5L-38 gas hydrate production research well. In *Scientific Results from the Mallik 2002 Gas Hydrate Production Research Well Program, Mackenzie Delta, Northwest Territories, Canada*; Geological Survey of Canada: Ottawa, ON, Canada, 2005.
20. Konno, Y.; Fujii, T.; Sato, A.; Akamine, K.; Naiki, M.; Masuda, Y.; Yamamoto, K.; Nagao, J. Key findings of the world's first offshore methane hydrate production test off the coast of Japan: Toward future commercial production. *Energy Fuels* **2017**, *31*, 2607–2616. [CrossRef]
21. Li, J.; Ye, J.; Qin, X.; Qiu, H.; Wu, N.; Lu, H.; Xie, W.; Lu, J.; Peng, F.; Xu, Z.Q.; et al. The first offshore natural gas hydrate production test in South China Sea. *China Geol.* **2018**, *1*, 5–16. [CrossRef]
22. Wu, N.; Li, Y.; Wan, Y.; Sun, J.; Huang, L.; Mao, P. Prospect of marine natural gas hydrate stimulation theory and technology system. *Nat. Gas Ind. B* **2021**, *8*, 173–187. [CrossRef]
23. Zhou, S.; Li, Q.; Lv, X.; Fu, Q.; Zhu, J. Key issues in development of offshore natural gas hydrate. *Front. Energy* **2020**, *14*, 433–442. [CrossRef]
24. Wu, S.; Wu, S.; Sun, J.; Li, Q.; Chen, J.; Chen, Y.; Zhou, X.; Khan, U. The Spatial Coupling of Fluid Pathways with Gas Hydrates and Shallow Gas Reservoirs: A Case Study in the Qiongdongnan Basin, South China Sea. *J. Mar. Sci. Eng.* **2024**, *12*, 659. [CrossRef]
25. Ren, J.; Cheng, C.; Xiong, P.; Kuang, Z.; Liang, J.; Lai, H.; Chen, Z.; Chen, Y.; Li, T.; Jiang, T. Sand-rich gas hydrate and shallow gas systems in the Qiongdongnan Basin, northern South China Sea. *J. Pet. Sci. Eng.* **2022**, *215*, 110630. [CrossRef]
26. Yang, L.; Wang, Z.; Shi, K.; Ge, Y.; Li, Q.; Leng, S.; Zhou, Y.; Zhang, L.; Zhao, J.; Song, Y. Upward migration of the shallow gas enhances the production behavior from the vertical heterogeneous hydrate-bearing marine sediments. *Energy* **2024**, *307*, 132612. [CrossRef]
27. Shi, K.; Feng, Y.; Gao, P.; Fan, Q.; Li, Q.; Leng, S.; Zhou, Y.; Zhang, L.; Zhao, J.; Liu, Y.; et al. Enhancing gas hydrate decomposition assisted by the shallow gas: Effects of interlayer permeability and depressurization strategies. *Fuel* **2024**, *374*, 132477. [CrossRef]

28. Zhao, Q.; Li, X.; Chen, Z.; Xia, Z.; Xiao, C. Numerical investigation of production characteristics and interlayer interference during co-production of natural gas hydrate and shallow gas reservoir. *Appl. Energy* **2024**, *354*, 122219. [CrossRef]
29. Jin, G.; Liu, J.; Su, Z.; Feng, C.; Cheng, S.; Zhai, H.; Liu, L. Gas production from a promising reservoir of the hydrate with associated and shallow gas layers in the low permeable sediments. *Energy* **2024**, *295*, 131079. [CrossRef]
30. Cheng, F.; Sun, X.; Li, Y.; Ju, X.; Yang, Y.; Liu, X.; Liu, W.; Yang, M.; Song, Y. Numerical analysis of coupled thermal-hydro-chemo-mechanical (THCM) behavior to joint production of marine gas hydrate and shallow gas. *Energy* **2023**, *281*, 128224. [CrossRef]
31. Wei, R.; Xia, Y.; Wang, Z.; Li, Q.; Lv, X.; Leng, S.; Zhang, L.; Zhang, Y.; Xiao, B.; Yang, S.; et al. Long-term numerical simulation of a joint production of gas hydrate and underlying shallow gas through dual horizontal wells in the South China Sea. *Appl. Energy* **2022**, *320*, 119235. [CrossRef]
32. Huang, H.; Huang, B.; Huang, Y.; Li, X.; Tian, H. Condensate origin and hydrocarbon accumulation mechanism of the deepwater giant gas field in western South China Sea: A case study of Lingshui 17-2 gas field in Qiongdongnan Basin. *Pet. Explor. Dev.* **2017**, *44*, 409–417. [CrossRef]
33. Wang, L.; Sun, Z.; Yang, J.; Sun, Z.; Zhu, J.; Zhuo, H.; Stock, J. Seismic characteristics and evolution of post-rift igneous complexes and hydrothermal vents in the Lingshui sag (Qiongdongnan basin), northwestern South China Sea. *Mar. Geol.* **2019**, *418*, 106043. [CrossRef]
34. Pei, J.; Luo, W.; Guo, S.; Lin, L.; Li, K. Discovery and petroleum geological significance of delta in the third member of Oligocene Lingshui Formation in southern Baodao Sag, Qiongdongnan Basin, South China Sea. *Pet. Explor. Dev.* **2024**, *51*, 337–350. [CrossRef]
35. Zhu, W.; Shi, H.; Huang, B.; Zhong, K.; Huang, Y. Geology and geochemistry of large gas fields in the deepwater areas, continental margin basins of northern South China Sea. *Mar. Pet. Geol.* **2021**, *126*, 104901. [CrossRef]
36. Yang, H.; Tang, H.; Ji, M.; Tian, Z.; Gao, Y. Formation and Evolution of the Late Triassic Granite Buried Hill in the Songnan Low Uplift, Qiongdongnan Basin. *Earth Sci.* **2025**, *50*, 2124–2143. [CrossRef]
37. Zhou, J.; Li, L.; Zhu, Z.; Wang, X.; Jin, J.; Wang, Y.; Zhang, Z. The distribution characteristics and the potential target of gas hydrate and shallow gas in the Qiongdongnan basin. *Acta Geol. Sin.* **2024**, *98*, 2630–2640.

Disclaimer/Publisher's Note: The statements, opinions and data contained in all publications are solely those of the individual author(s) and contributor(s) and not of MDPI and/or the editor(s). MDPI and/or the editor(s) disclaim responsibility for any injury to people or property resulting from any ideas, methods, instructions or products referred to in the content.